Journal of Food Bioactives
International Society for Nutraceuticals and Functional Foods
Original Research
J. Food Bioact. 2026;33:38–53

Effects of highly bioavailable 2,5-diketopiperazines in standardized extract of cultured *Lentinula edodes* mycelium (ECLM) on phagocytosis and inflammatory mediators production by J774A.1 macrophages

Ann Elaine D.S. Wagan, Atsuya Nagao, Sri Wijanarti, Satoshi Miyauchi, Tomoko T. Asai and Kenji Sato*

Division of Applied Biosciences, Graduate School of Agriculture, Kyoto University, Kyoto, Japan
*Corresponding author: Division of Applied Biosciences, Graduate School of Agriculture, Kyoto University, Kyoto Japan. E-mail: kenji-sato6213@gmail.com
DOI: 10.26599/JFB.2026.95033438
Received: October 21, 2025; **Revised received & accepted:** December 9, 2025
Citation: Wagan, A.E.D.S., Nagao, A., Wijanarti, S., Miyauchi, S., Asai, T.T., and Sato, K. (2026). Effects of Highly Bioavailable 2,5-Diketopiperazines in Standardized Extract of Cultured *Lentinula edodes* Mycelium (ECLM) on Phagocytosis and Inflammatory Mediators Production by J774A.1 Macrophages. J. Food Bioact. 33: 38–53.

Abstract

A standardized extract of cultured *Lentinula edodes* mycelia (ECLM) has been reported to enhance innate and acquired immunity and suppress chronic inflammation. The present study revealed that the aqueous extract of ECLM significantly enhanced the phagocytic activity of J774A.1 macrophages. After fractionation, 23 distinct 2,5-diketopiperazines (DKPs) were identified in the active fraction, of which 12 were detected at concentrations ≥1 μmol/kg or L in various samples from rats after oral administration of ECLM at 0.5 and 1.0 g/kg. These bioavailable DKPs did not suppress phagocytosis in LPS-stimulated macrophages, whereas DKPs significantly suppressed LPS-induced NO and IL-6 productions. In the absence of LPS, these DKPs significantly enhanced phagocytosis in macrophages to levels similar to those achieved by the calcium sensing receptor (CaSR) allosteric agonist R-568, which was partially abolished by the CaSR allosteric antagonist NPS-2143. These facts indicate that DKPs in ECLM have dual roles in promoting innate immune responses without inducing proinflammatory responses, possibly via allosteric CaSR activation.

Keywords: AHCC; Diketopiperazines; Macrophage; Phagocytosis; CaSR.

1. Introduction

Mushroom mycelia have a root-like structures that typically grows in soil or wood. A standardized extract of cultured *Lentinula edodes* mycelia (ECLM) is a functional food ingredient obtained through the standard culture process of the mycelia (Shin et al., 2019). ECLM has been widely recognized for its therapeutic potential as a complementary and alternative medicine (CAM) for patients with hepatitis, cancer, and infectious diseases (Matsui et al., 2002; Kawaguchi, 2009; Yin et al., 2010; Smith et al., 2022). A human cohort study reported that ECLM ingestion improved the survival periods and recurrence periods of patients with hepatic carcinoma who had undergone surgery (Matsui et al., 2002). Recently, ECLM has been shown to be effective in supporting the host immune system to eliminate persistent human papilloma virus (HPV) infections (Smith et al., 2022). In addition, ECLM supplementation enhanced the innate immune response to primary influenza infection (H1N1) (Ritz et al., 2006).

It has been reported that ECLM contains polysaccharides, such as acylated α-1,4 glucans, and amino acids, peptides, vitamins, and minerals (Sato and Kashimoto, 2017). Several animal and human studies have reported that ECLM exerts immune-enhancing ef-

fects on monocytes, dendritic cells (DC), T cells, and natural killer (NK) cells, and promotes anti-inflammatory activity (Daddaoua et al., 2007; Terakawa et al., 2008; Lee et al., 2012; Kogiso et al., 2015; Chowdhury et al., 2019; Shin et al., 2019; Singh et al., 2023). These activities have been linked to the beneficial effects in patients with cancer and viral infections. The immune-enhancing effects are suggested to be mediated by partially acetylated α-glucan via toll-like receptors (TLRs); however the exact bioactive compounds responsible for the dual immune-enhancing and anti-inflammatory activities remain unknown (Mallet et al., 2016).

The innate immune system serves as the body's first line of defense and plays a vital role in recognizing and eliminating pathogens (Wu et al., 2024). However, only a few studies have specifically focused on the role of ECLM in modulating macrophages, which are central players in innate immunity (Daddaoua et al., 2013). Derived from circulating monocytes, macrophages differentiate into subtypes, such as M1 and M2, each with distinct functions. M1 macrophages, in particular, are known for their ability to eliminate pathogens, virus-infected cells, and malignant cells through phagocytosis, a critical immune process for eliminating harmful pathogens or abnormal cells (Chen et al., 2023). Macrophages also act as mediators between the innate and adaptive immune systems, influencing T and NK cells through antigen presentation and the production of cytokines and low–molecular weight signaling molecules such as nitric oxide (NO) (Chen et al., 2023; Dash et al., 2024). However, during persistent immune activation, macrophages can contribute to chronic inflammation through the overproduction of NO and proinflammatory cytokines such as interleukin-6 (IL-6), interleukin 1β (IL-1β) and tumor necrosis factor-α (TNF- α) (Kim and Lee, 2025). Therefore, modulating macrophage functions—particularly enhancing phagocytic activity while regulating their inflammatory response—through food-derived bioactives, such as those in ECLM, presents a promising strategy for preventing non-communicable and communicable diseases. However, the effects of ECLM on macrophage phagocytosis have not been examined, although its anti-inflammatory activity has been reported (Daddaoua et al., 2007; Tanaka et al., 2014).

Our preliminary experiments showed that the aqueous extract of ECLM enhanced the phagocytosis of beads in J774A.1 macrophage-like cells. The objectives of this study were to identify the bioactive compounds responsible for the phagocytosis-enhancing activity of ECLM and to evaluate their bioavailability and effects on lipopolysaccharides (LPS)-stimulated production of inflammatory mediators such as NO and IL-6. This study provides important insights into the potential of ECLM-derived bioactive compounds as immunomodulators and supports their application in functional foods and nutraceuticals.

2. Materials and methods

2.1. Sample and reagents

Standardized ECLM was obtained from Amino Up (Sapporo, Hokkaido, Japan). This product, in the powder form, is commercially available as AHCC®. Fetal bovine serum (FBS) was obtained from Biowest (Nuaillé, France). Penicillin–streptomycin mixture, trypsin solution (2.5 g/L in 1 mM EDTA), RPMI 1640 medium, and HPLC-grade acetonitrile were obtained from Nacalai Tesque (Kyoto, Japan). Calcium-sensing receptor (CaSR) allosteric antagonist (NPS-2143) and agonist (R-568) were purchased from Selleckchem (Houston, TX, USA). Gentamicin was obtained from Gibco-Thermo Fisher Scientific (Waltham, MA, USA). Mouse IL-6 ELISA kit was purchased from Invitrogen-Thermo Fisher Scientific (Waltham, MA, USA). A mixture of amino acid standards (Type H), phenyl isothiocyanate (PITC), trypan blue staining solution, and LPS were purchased from Fujifilm Wako Pure Chemical (Osaka, Japan). 9-Fluorenylmethyloxycarboxynyl (Fmoc)-amino acids, and Fmoc-amino acid–bound resins (Wang resin, Alko resin, and Trt(2-Cl)-resin) were purchased from Watanabe Chemical Industries (Hiroshima, Japan). All other reagents were of analytical grade or higher. Purified water from a Mili-Q® system (Merck Millipore, Darmstadt, German) was used for the study.

2.2. Fractionation of compounds in the aqueous extract of ECLM

ECLM was mixed with water to yield a 10% (w/v) suspension and vortexed for a few minutes and centrifuged at 10,000 × *g* for 5 min at 5 °C. The supernatant was considered the aqueous extract of ECLM. The aqueous extract was then mixed with three times the volume of ethanol, making it a 75% (v/v) ethanol system. The mixture was allowed to settle for 1 h, and the soluble and precipitated fractions were separated using centrifugation 10,000 × *g* for 5 min at 5 °C. Compounds in the 75% ethanol-soluble fraction were further fractionated using a strong cation exchanger, AG 50W- ×8 resin (hydrogen form; Bio-Rad Laboratories, Hercules, CA, USA) according to a previously described method (Aito-Inoue et al., 2006). The resin was packed into a spin column (Ultrafree® MC-SV, 5-µm pore size, Merck Millipore) and equilibrated with 50% acetonitrile–water solution. An aliquot of the ethanol-soluble fraction (200 µL) was passed through a spin column. The non-adsorbed fractions were collected and designated as AG50 non-adsorbed fractions. After washing the spin column with 50% methanol (200 µL), the bound compounds were eluted with 200 µL of 7.5 M ammonium hydroxide containing 50% methanol (five times) and used as the AG50 adsorbed fraction.

The 75% ethanol precipitate was dissolved in water at the same initial volume as the aqueous extract. The AG50 non-adsorbed and adsorbed fractions of the 75% ethanol-soluble fraction were spin dried and reconstituted in water at the same initial volume as the aqueous extract.

2.3. Identification of compounds in the AG50 non-adsorbed fraction

The AG50 non-adsorbed fraction was clarified by filtration through a 0.45-µm pore size filter (Cosmonice, 4 mm i.d., Nacalai Tesque). An aliquot of the filtrate (10 µL) was subjected to liquid chromatography-tandem mass spectrometry (LC-MS/MS) using an LCMS-8040 (Shimadzu, Kyoto, Japan). The compounds in the samples were separated by reverse-phase HPLC (RP-HPLC) using an ODS-3 column (2.1 mm × 250 mm, GL Science, Tokyo, Japan). The mobile phase consisted of solvent A (0.1% formic acid) and solvent B (0.1% formic acid in 80% acetonitrile). The gradient elution program was as follows: 0–15 min, B 0–50%; 15–20 min, B 50–100%; 20–22 min, B 100%; 22–22.1 min, B 100–0%; 22.1–30 min, B 0%. The flow rate was maintained at 0.2 mL/min and the column temperature was set at 40 °C. Detection of compounds in the effluent was carried out by a total ion scan in the positive ion mode of the MS, scanning the following range of mass-to-charge ratios (*m/z*): 100–150, 150–200, 200–225, 225–250, 250–275, 275–300, 300–400, 400–500, and 500–1,000. Precursor ions corresponding to major peaks were further analyzed in product ion scan mode at collision energies of –15, –25, and –35 eV using same elution conditions. The structure of the amino terminal–

blocked linear peptides was estimated based on *m/z* of the precursor ions, immonium ions, and peptide-derived product ions (a, b, c and x, y, z ions) (Papayannopoulos, 1995). Structures of cyclic peptides (diketopiperazines, DKPs) were estimated based on *m/z* of product ions, immonium ions, and DKP-specific fragment ions (*m/z* 98.0, 113.0, 125.0) (Nagao et al., 2024).

2.4. Synthesis of peptides and DKPs

Proline-based DKPs identified in the ECLM were synthesized according to the method described by Nagao et al. (2024) using an automated solid-phase peptide synthesizer (PSSM-8, Shimadzu, Japan) based on Fmoc chemistry. Briefly, proline-based DKPs were efficiently generated via cyclization by cleaving the peptide from X-Pro-Wang/Alko-resins using trifluoroacetic acid (TFA) , where X represents any other amino acid residue. Non-proline–based DKPs were prepared from linear dipeptides with methyl-esterified carboxyl groups. The carboxyl groups of the linear peptides were methyl-esterified by catalysis of AG50 (Nagao et al., 2024). DKPs were generated by heating the methyl-esterified peptides at 98 °C in *tert*-butanol for 3 h.

DKPs were purified using RP-HPLC on a Cosmosil MS-II column (10 mm × 250 mm, Nacalai Tesque). The binary mobile phase system consisted of solvent A (0.1% formic acid) and solvent B (0.1% formic acid in 80% acetonitrile). The gradient elution program was: 0–20 min, B 0–50%; 20–30 min, B 50–100%; 30–35 min, B 100%; 35–35.1 min, B 100–0%; 35.1–45 min, B 0%. Flow rate was 2 mL/min, and column temperature was maintained at 45 °C.

Purified DKPs were quantified after hydrolysis with 6 M HCl at 150 °C under vacuum for 1 h. Amino acids in the hydrolysates were derivatized with PITC according to the method described by Bidlingmeyer et al. (1984) and analyzed using RP-HPLC (Nagao et al., 2024) to determine the concentration of each synthesized DKP. Stock solutions were then diluted to working concentrations of 1, 10, and 100 µM. When added to the culture medium, the final concentrations of each DKP for treatment were 0.01, 0.1, and 1 µM, respectively. γ -glutamyl-valine (γ-EV) was also prepared following the method described by Rahmadian et al. (2025).

2.5. Animal experiments

Animal experiments were conducted at the Louis Pasteur Center for Medical Research (Shimadzu, Kyoto, Japan) in accordance with the standards established by the National Institutes of Health's Guide for the Care and Use of Laboratory Animals. All experimental procedures were approved by the Animal Care Committee of the Louis Pasteur Center for Medical Research (approval no. 2023-1). Male Wistar/ST rats (6-week old; 150–170 g body weight) were purchased from Japan SLC (Shimadzu, Kyoto, Japan) and acclimatized under controlled environmental conditions (24–26 °C, 40–60 % humidity, 12-h light/dark cycle) for 1 week. During the acclimatization period, rats were fed the MF (maintenance formula/feed) diet (12 mmφ pellets, 359 kcal/100 g, Oriental Yeast, Tokyo, Japan) and had free access to water. Rats (average body weight, 168 g) were fasted overnight for 16 h before the experiment. Distilled water was used as a vehicle control (n = 3). ECLM was prepared as a 10% (w/v) aqueous extract, as described in Section 2.2, administered orally at doses of 0.5 g and 1.0 g/kg body weight of rats. Rats were anesthetized using isoflurane, followed by dissection 30, and 60 min after administration of vehicle or ECLM (n = 3 per group). Blood was collected from the portal and abdominal vein (inferior vena cava), and plasma was obtained using centrifugation (800 × *g*, 10 min, 4°C) in the presence of heparin. The stomach and small intestine were collected, and their luminal contents were flushed with 10 mL of PBS. The collected plasma and luminal effluents from stomach and small intestine were mixed with three times the volume of ethanol, and the supernatants were collected after centrifugation (12,000 × *g*, 10 min, 5 °C) and stored at –80 °C until analysis. The small intestine was divided into three equal-length sections: anterior, mid, and posterior parts. Approximately, 100 mg of tissue from the center of each section was excised and homogenized with an equal volume of PBS (v/w) using a BioMasher II (Nippi, Tokyo, Japan). After thorough homogenization, three times the volume of ethanol were added to each homogenate. The mixture was vortexed and incubated on ice for 10 min, followed by centrifugation at 12,000 × *g* for 10 min at 5 °C. The resulting supernatants were carefully collected and stored at −80°C until further analysis.

2.6. Quantification of DKPs

DKPs levels in ECLM and in blood and tissue samples from rat were determined using LC-MS/MS in the multi-reaction monitoring (MRM) mode. The synthesized DKPs were used to optimize the MRM conditions using LabSolutions LCMS Ver.5.5 (Shimadzu). The elution conditions were the same as those used for the total ion scan mode of the LC-MS/MS described in Section 2.3. Aliquots of the 75% ethanol supernatants (100 µL) from plasma, luminal contents of the stomach and small intestine, and tissue extracts were spin-dried and dissolved in water (100 µL). A 10-µL aliquot of each sample was injected into the LC-MS/MS.

2.7. Cell culture

Frozen J774A.1 cells in a cryovial were obtained from the Japanese Collection of Research Bioresources Cell Bank (JCRB, Osaka, Japan) and stored at –80 °C. The cells were thawed in a water bath at 37 °C and maintained in a cell culture dish (100 mm i.d.) in RPMI 1640 medium supplemented with 10% FBS, and 0.1% of the following antibiotic stock solutions: penicillin–streptomycin mixture, and 10 mg/mL gentamicin. Cell cultures were maintained in a humidified incubator at 37 °C with 5% CO_2 until 70–80% cell confluence was achieved. Cells were then harvested by trypsinization using four fold–diluted trypsin solution with PBS for 3 min, followed by centrifugation at 1,000 × *g* for 5 min. The cell pellet was resuspended in serum-free RPMI 1640 medium. To count live cells, a 50-µL aliquot of the cell suspension was collected and an equal volume of trypan blue staining solution (0.4% trypan blue in PBS) added. Non-stained cell numbers were counted using a hemocytometer. In the following experiments, the FBS was used after removing low–molecular weight compounds <6 kDa using size exclusion chromatography with an Econo-Pac 10DG (Bio-Rad Laboratories) column, according to the method described by Asai et al. (2020), which is referred to as SEC-FBS in the following section.

Prior to the NO production and phagocytosis experiments, effects of LPS (0.1, 1.0, 10 µg/mL) and DKPs (1 µM) on viability of J774A.1 were examined. Using a 96-well microplate, 100 µL of complete medium containing the SEC-FBS and LPS (0.0, 0.2, 2.0, 20 µg/mL) in the presence and absence of a mixture of DKPs (1 µM of each DKP; cyclo-Gly-Pro [cGP], cyclo-Ser-Pro [cSP], cyclo-Thr-Pro [cTP], cyclo-Asn-Pro [cNP], cyclo-Asp-Pro [cDP], cyclo-Ala-Pro [cAP], cyclo-Pro-Pro [cPP], cyclo-Ala-Val [cAV],

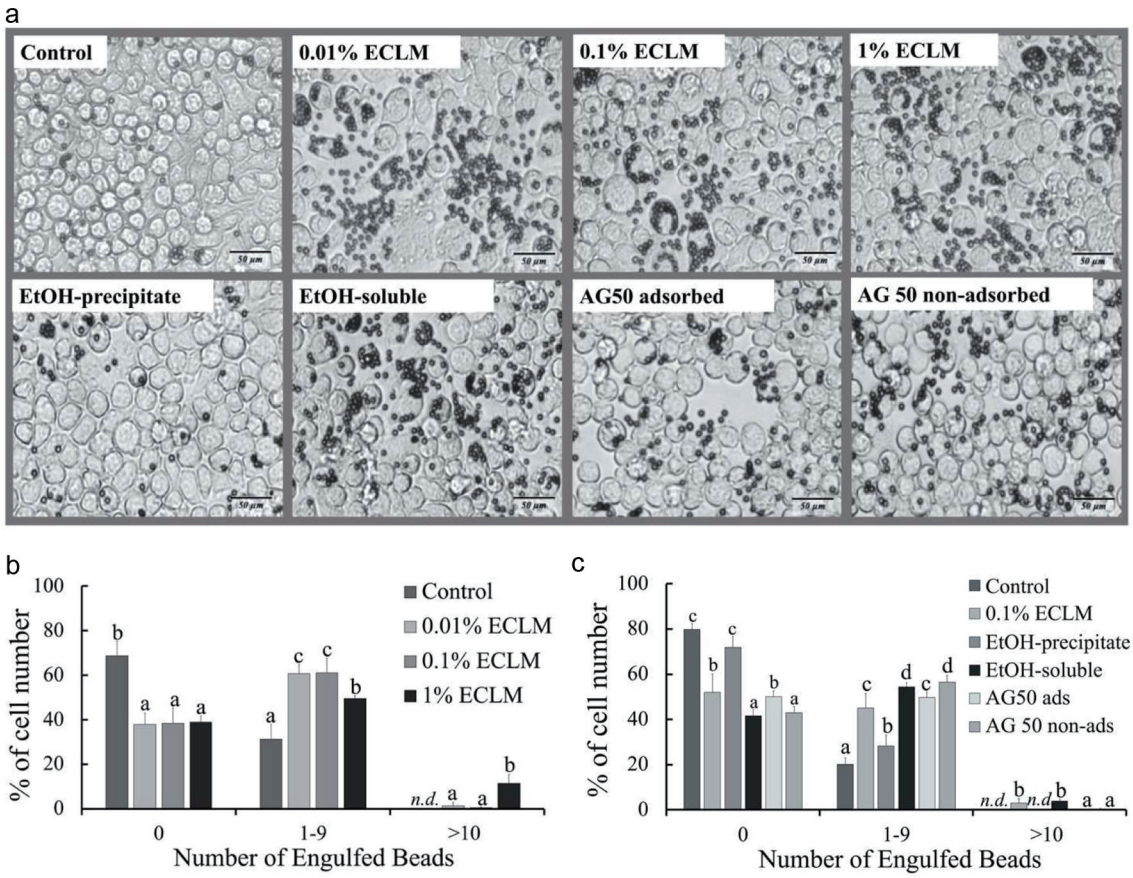

Figure 1. Effects of aqueous extract of cultured *Lentinula edodes* mycelia (ECLM) and its fractions on the phagocytic activity of J774A.1 cells. (a) Representative images of J774A.1 cells incubated with beads and samples for 24 h. (b and c) Percentage of cells engulfing 0, 1–9, or >10 beads. Data are shown as mean ± SD. Different letters (anc) indicate significant differences between groups (Tukey's post hoc, $p < 0.05$). *n.d*. represents not detected; EtOH, ethanol; AG50-ads, adsorbed, AG50 non-ads, non-adsorbed

cyclo-Ile-Pro [cIP], cyclo-Leu-Pro [cLP], cyclo-Val-Pro [cVP], and cyclo-Asp-Leu [cDL]) was added to each well. Then, 5×10^5 cells in 100 µL of medium without LPS and DKPs were added to all wells and mixed gently. After 24 h of incubation, live cells were manually counted as described above. All tests were performed in triplicate. Viability of cells treated with the DKP mixture was also examined by the water-soluble tetrazolium salt (WST)-8 method using a CCK-8 reagent (Dojindo Laboratories, Kumamoto, Japan). The same number of cells was incubated for 24 h in the medium containing the same DKP mixture at a final concentration of 0.0, 0.01, 0.1, 1.0, and 10.0 µM of each DKP. Cell numbers were estimated from the standard curve using absorbance at 450 nm and known cell numbers.

2.8. Phagocytosis assay

The effect of the aqueous extract of ECLM and its fractions on phagocytosis in J774A.1 was examined. J774A.1 suspension (500 µL) in the complete medium containing 10% SEC-FBS was seeded in tissue culture plates (0.25×10^6 cells/well in a 24-well plate) and incubated overnight at 37 °C to ensure full adherence prior to treatment. After the overnight incubation, the cell medium was replaced with 500 µL of the complete medium containing 10% SEC-FBS, sample, and latex beads suspension (3.0 µm mean particle size, LB30-1mL, Sigma-Aldrich, Merck), resulting in a final concentration of 0.5 µL/mL latex beads in the medium. After a 24-h incubation, phagocytosis was terminated by washing cells five times with cold PBS, and cells were fixed using 10% paraformaldehyde. Cell images were captured using an Olympus IX73 inverted microscope equipped with the cellSens Standard software (Olympus, Tokyo, Japan). The number of cells containing beads was manually counted. Aqueous extracts of the ELCM, ethanol-soluble and precipitate fractions, and AG50 adsorbed and non-adsorbed fractions of the ethanol-soluble fraction were used as samples. All samples were dissolved into water, as mentioned previously. Sample stock solutions were then added to the medium. The concentration of each sample in the medium is shown in the legend of Figure 1, presented in terms of the amount of ECLM used to prepare each fraction.

Next, the effects of mixtures and individual DKPs in the presence of LPS on phagocytosis in J774A.1 were examined. To the medium, LPS and DKPs mixtures were added to achieve a final concentration of 0.1 µg/mL LPS, and 0.1 and 1.0 µM of each DKP. A J774A.1 cell suspension (300 µL) in the complete medium containing 10% SEC-FBS and DKPs mixture in the presence and absence of LPS was seeded in tissue culture plates (0.125×10^6 cells/well in a 48-well plate) and incubated overnight at 37 °C for 24 h to prime the cells. Then, the medium was replaced with 300 µL of fresh complete medium containing beads, giving a final

concentration of 0.5 µL/mL of beads in the medium, and incubated for a suitable time. The composition of the DKP mixture was determined based on bioavailability, hydrophobicity, and the presence of proline residue. The constituent DKPs in the mixtures are shown in the figure legends. Furthermore, in the absence of LPS, effects of each DKP on phagocytosis in the absence and presence of the CaSR allosteric antagonist, NPS-2143, were examined. The CaSR allosteric agonist, R-568, was also added to the medium in the absence of DKPs. Another food-derived peptide, γ-EV, was added to the medium in the presence or absence of NPS-2143. Phagocytosis was terminated as described earlier. Images of fixed cells were analyzed using a cell counting software (ITAH601K-TU22C0010; ITAGE, Nagoya, Japan). The software detected the numbers of beads inside the cells, but not those outside, and enabled the quantification of cell numbers with 0–9 beads and those with more than 10.

2.9. NO production

To evaluate NO production, 300 and 500 µL of the cell suspension in complete medium were seeded in cell culture plates; 0.125×10^6 cells/well in a 48-well plate or 0.25×10^6 cells/well in a 24-well plate, respectively, and incubated overnight at 37 °C to ensure full adherence prior to treatment. J774A.1 cells were stimulated with the fresh complete medium containing 10% SEC-FBS, 0.1 µg/mL LPS in the presence or absence of DKP mixtures and each DKP. Culture media were collected at suitable intervals. NO concentrations in the media were quantified by measuring the nitrite content using a Griess reagent (0.1% *N*-1-naphthylethylenediamine dihydrochloride and 1% sulfanilamide in 5% phosphoric acid) and incubating at room temperature for 10 min. Absorbance at 550 nm was measured using a microplate reader. Sodium nitrite ($NaNO_2$) served as the standard.

2.10. IL-6 protein levels

Cell culture supernatants were collected from J774A.1 macrophages treated with individual DKPs in the presence and absence of LPS. Protein levels of IL-6 in the medium was quantified using commercially available mouse IL-6 ELISA kit according to the manufacturer's instructions. Briefly, ELISA plates were coated with 100 µL/well of capture antibody (1×) and incubated overnight at 4°C without shaking. Following coating, wells were washed twice with 400 µL/well of wash buffer, allowing 10–15 seconds of soaking per wash, and excess buffer was removed. Wells were then blocked with 200 µL/well of ELISA diluent (1×) and incubated at room temperature for 1 h. Standard solution was prepared, and two-fold serial dilutions were performed to generate a 7-point standard curve plus a blank. After blocking, 100 µL of each standard and sample solution was added to designated wells, and the plates were sealed and incubated on a microplate shaker at 400 rpm for 2 h at room temperature. Following incubation, wells were washed four times and 100 µL of detection antibody (1×) was added to each well. Plates were then incubated on a shaker at 400 rpm for 1 hour at room temperature. Subsequently, wells were washed five times before adding 100 µL of enzyme solution (1×) per well, followed by incubation on a shaker at 400 rpm for 30 min at room temperature. After five additional washes, 100 µL of TMB substrate solution (1×) was added to each well and incubated at room temperature for 15–30 min without shaking, until the highest standard developed a dark blue color. The reaction was stopped by adding 100 µL of stop solution (1×) to each well, and absorbance was measured at 450 nm, with 620 nm as reference for background subtraction when available. Protein concentrations of IL-6 in the samples were determined from the standard curve.

2.11. Statistical analyses

Animal experiment, NO and IL-6 assays were performed in triplicates (n=3). For phagocytosis analysis, three wells were used for each condition. An average of 10 images was captured from each well. The average numbers of cells with 0–9 and more than 10 beads from 10 images were used as the values for each well. Data are presented as average ± standard deviation (SD). Statistical comparisons were performed using one-way analysis of variance (ANOVA) followed by Tukey's multiple comparisons test to evaluate the differences between groups. Comparisons between two groups were performed using the *t*-test. The significance threshold was set at $p < 0.05$. All analyses were performed using a GraphPad Prism (version 6.04, GraphPad Software, San Diego, CA, USA).

3. Results

3.1. Effects of aqueous extract of ECLM on phagocytosis

Figure 1a shows representative images of J774A.1 cells incubated with beads and the aqueous extract of ECLM or its fractions for 1 day. As mentioned earlier, the sample concentrations in the medium are presented in terms of the amount of ECLM used to prepare each fraction. Addition of the aqueous extract at 0.01 % in the medium significantly increased the number of cells engulfing 1–9 and >10 beads compared with the control group (Figure 1b). At doses of 0.1 and 1.0 %, the total number of cells engulfing beads was not significantly different compared with that at the 0.01 % dose; however, at 1.0 %, the number of cells engulfing more than 10 beads was significantly higher compared with that of the other doses (Figure 1b). These findings indicated that the aqueous extract of ECLM can enhanced phagocytosis in J774A.1.

To estimate the type of compounds responsible for this effect, compounds in the aqueous extract of ECLM were fractionated by ethanol precipitation, followed by solid-phase extraction using a strong cation exchanger. As shown in Figure 1c, the 75% ethanol-soluble fraction significantly increased the number of cells engulfing beads, whereas the ethanol precipitate did not, which indicates that low–molecular weight compounds, rather than high–molecular weight proteins and polysaccharides, are responsible for the phagocytosis enhancing effect of ECLM. The strong cation exchange resin (AG50) non-adsorbed fraction of the 75% ethanol-soluble sample also showed a more significant increase in the number of cells engulfing the beads compared to the adsorbed fraction. This result indicated that the compounds in the non-adsorbed fraction were mainly responsible for the enhanced phagocytic activity of cells treated with the aqueous extract of ECLM.

3.2. Identification of compounds in the non-adsorbed fraction

Figure 2a shows the total ion chromatograms of the AG50 non-adsorbed fraction at different scan ranges of mass-to-charge ratio (*m/z)*. Peaks marked with numbers in Figure 2a were further analyzed using product ion scanning to estimate their structures. Figure 3a shows representative spectrum assignment of product

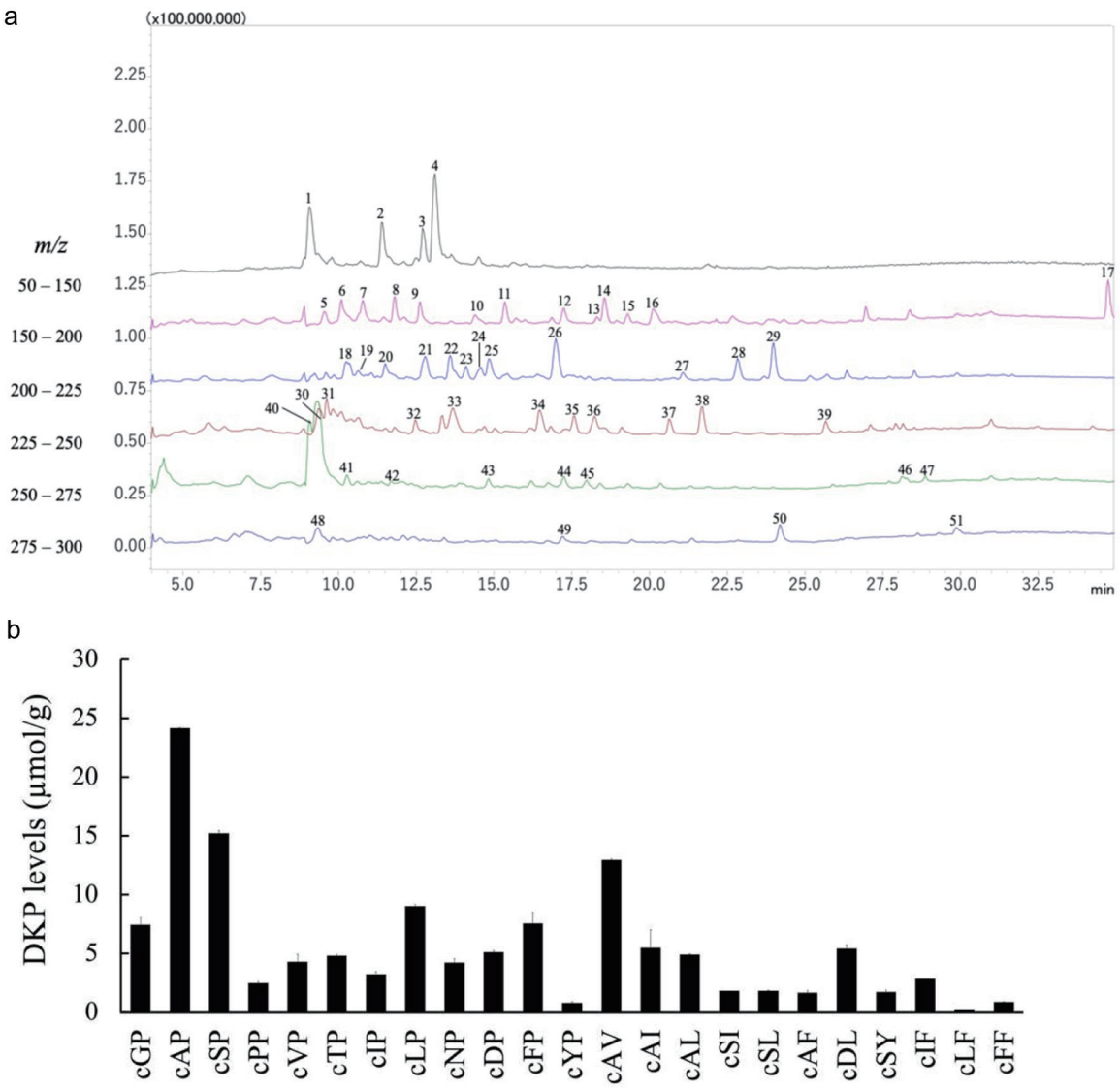

Figure 2. Identification and quantification of 2,5-diketopiperazines (DKPs) in the ECLM. (a) Mass spectrometry (MS) chromatograms of compounds in the AG50 non-adsorbed fraction of ECLM. Compounds were detected by total ion scan in positive ion mode, covering mass-to-charge ratio (*m/z*) ranges of 100–150, 150–200, 200–225, 225–250, 250–275, and 275–300. Peaks labeled 1–51 were further analyzed by product ion scan to estimate their structures. (b) Concentrations of DKP in ECLM (µmol/g). DKPs were quantified using LC-MS/MS in MRM mode. Data are shown as mean ± SD (n = 3). DKPs: cyclo-Gly-Pro [cGP], cyclo-Ala-Pro [cAP], cyclo-Ser-Pro [cSP], cyclo-Pro-Pro [cPP], cyclo-Val-Pro [cVP], cyclo-Thr-Pro [cTP], cyclo-Ile-Pro [cIP], cyclo-Leu-Pro [cLP], cyclo-Asn-Pro [cNP], cyclo-Asp-Pro [cDP], cyclo-Phe-Pro [cFP], cyclo-Tyr-Pro [cYP], cyclo-Ala-Val [cAV], cyclo-Ala-Ile [cAI], cyclo-Ala-Leu [cAL], cyclo-Ser-Ile [cSI], cyclo-Ser-Leu [cSL], cyclo-Ala-Phe [cAF], cyclo-Asp-Leu [cDL]), cyclo-Ser-Tyr [cSY], cyclo-Ile-Phe [cIF], cyclo-Leu-Phe [cLF], and cyclo-Phe-Phe [cFF],

ions. A summary of the estimated structures of each peak, based on *m/z* of precursor and product ions, is shown in Table 1. Overall, 23 DKPs; 11 pyroglutamyl peptides; and a few formyl, acetyl, and lactoyl amino acids were identified. In our preliminary experiments, DKPs, rather than pyroglutamyl peptides, showed stronger activity in enhancing the phagocytosis of J774A.1. Thus, we focused on DKPs in subsequent phagocytosis analyses. The presence of the DKPs in the ECLM, listed in Table 1, was confirmed by comparing the retention times and *m/z* of the product ions of synthetic DKPs using LC-MS/MS in MRM mode. Figure 3b shows MS chromatograms for standard cAP and portal vein blood samples 30 min after administration of ECLM.

Figure 2b shows the DKP contents in ECLM. ECLM contains not only Proline (Pro) -containing DKPs, such as cAP, cSP, and cLP but also non-Pro DKPs such as cAV.

3.3. Bioavailability of diketopiperazines in rat

Most DKPs in ECLM, except for cFF and cI/LF, were significantly increased in the luminal content of the stomach 30 and 60 min after administration of the aqueous extract of ECLM at both 0.5 and 1.0 g/kg body weight (data not shown). Figure 4 shows the concentrations of DKPs in the mid-section of small intestine tissue, portal vein blood, and abdominal vein blood before and 30 and 60 min after the administration of ECLM at 0.5 and 1.0 g/kg

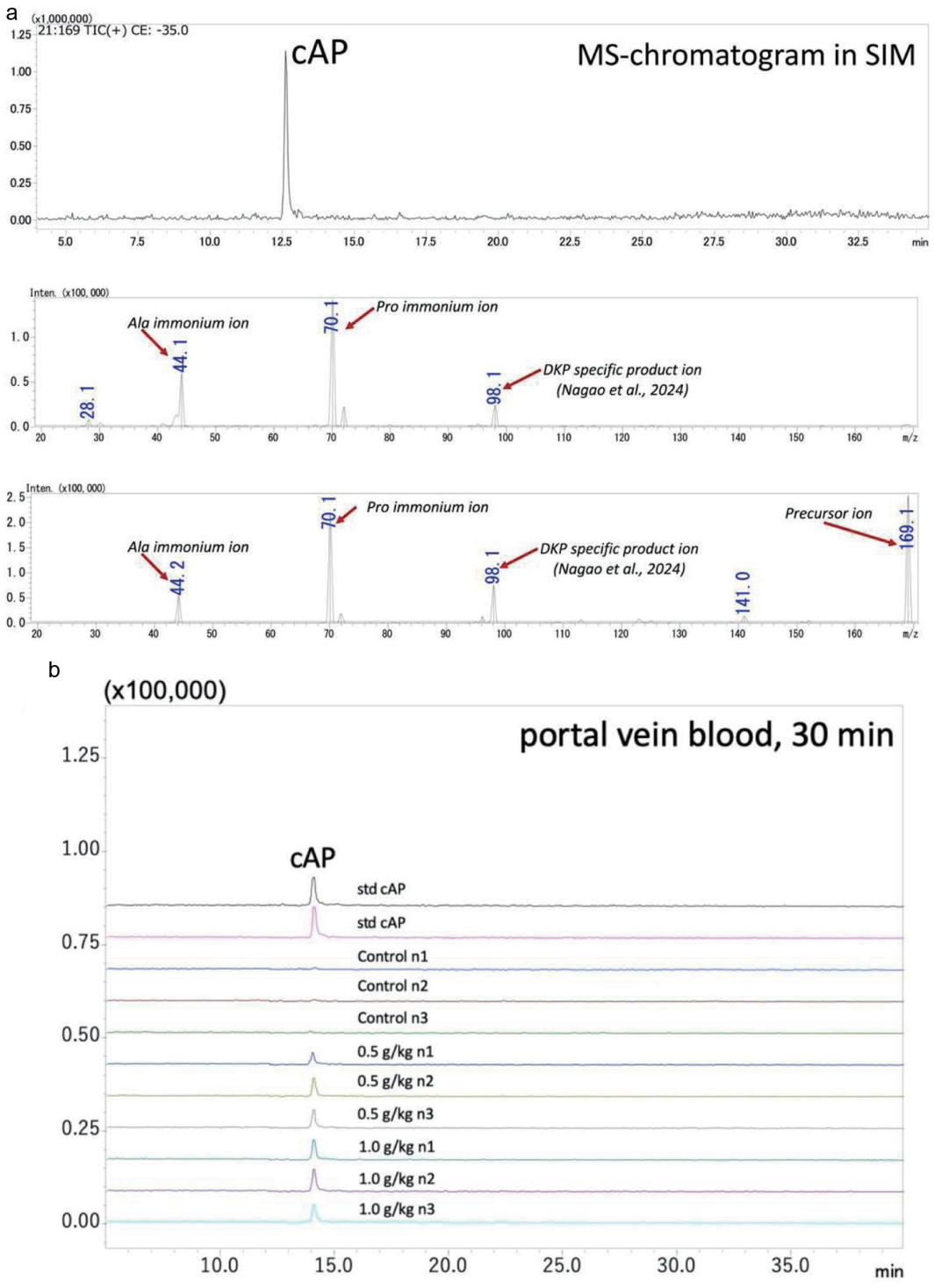

Figure 3. MS chromatogram of representative DKP (cAP) and spectra of product ions. (a) MS chromatogram of cAP in aqueous extract of ECLM in single ion monitoring mode (*m/z*=169) and spectra of product ions at collision energy −35 eV and −15 eV. (b) MS chromatograms in MRM mode of standard cAP (std) and plasma of rats portal blood 30 min after administration of 0.5 and 1.0 g/kg body weight of ECLM (n=3). std cAP means standard cyclo-Ala-Pro;

body weight. Among the 23 DKPs identified in the ECLM aqueous extract, nine DKPs (cDP, cNP, cGP, cSP, cTP, cAP, cPP, cAV, and cDL) were present at concentrations higher than 1 µmol/kg in the mid-section of small intestine 30 and 60 min after administration of either dose. Further, nine other DKPs (cGP, cSP, cTP, cAP, cPP, cAV, cIP, cLP, and cVP) exhibited high bioavailability (>1 µM) in portal vein blood. In abdominal vein blood, the DKPs with high bioavailability largely reflected those in portal vein blood, except

Table 1. Summary of estimated structure of each peak based mass-to-charge ration (*m/z*) of precursor and product ions

Peak	Precursor ion (*m/z*)	Estimated structure	Product ions (*m/z*)
1	130.1	pyroGlu	28.3(pyroGlu*), 41.2(pyroGlu*), 56.2(pyroGlu*), 84.1(pyroGlu*)
2	145.0	*cannot be assigned to peptide*	43.1, 71.1, 99.1, 127.1, 145.1
3	127.0	*cannot be assigned to peptide*	43.1, 53.0, 81.0, 109.0, 127.0
4	109.0	*cannot be assigned to peptide*	27.0, 53.0, 81.0, 109.0
5	190.1	N-acetyl-pyro Glu	43.2 (acetyl*), 56.2(pyroGlu*), 84.2 (pyroGlu*), 102 (Glu*), 130.1, 148.1, 172.1
6	185.1	cyclo (-Ser-Pro); cSP	60.2(Ser*), 70.1(Pro*), 98.0, 125.1(derived from diketopiperazine rings)
7	155.1	cyclo (-Gly-Pro); cGP	30.2(Gly*), 70.1(Pro*), 98.0, 125.1(derived from diketopiperazine rings)
8	199.1	cyclo (-Thr-Pro); cTP	70.2(Pro*), 74.1(Thr*), 98.2, 125.1, 153.1(derived from diketopiperazine rings)
9	169.1	cyclo (-Ala-Pro); cAP	44.1(Ala*), 70.2(Pro*), 98.1, 113.1 (derived from diketopiperazine rings)
10	158.1	N-formyl pyro Glu	28.9 (formyl*), 28.2(pyroGlu*), 41.4(pyroGlu*), 56.2(pyroGlu*), 84.1(pyroGlu*)
11	171.1	cyclo (-Ala-Val); cAV	44.1(Ala*), 72.1(Val*), 98.1 (derived from diketopiperazine rings)
12	197.1	cyclo (-Val-Pro); cVP	72.1(Val*), 70.1(Pro*), 98.0, 153.8 (derived from diketopiperazine rings)
13	185.1	cyclo (-Ala-Ile); cAI	44.1(Ala*), 86.2 (Ile*), 113.6 (derived from diketopiperazine rings)
14	195.1	cyclo (-Pro-Pro); cPP	70.2(Pro*), 70.2(Pro*), 98.1(derived from diketopiperazine rings)
15	185.1	cyclo (-Ala-Leu); cAL	44.1(Ala*), 86.2 (Leu*), 113.6 (derived from diketopiperazine rings)
16	194.1	N-formyl-Phe	29.4 (formyl*), 91.0 (Phe*), 108, 120.1 (Phe*) 136.2, 166.2, 173.2
17	174.1	*cannot be assigned to peptide*	29.1, 42.1, 55.7, 67.1, 77.4, 82.0, 84.1, 128.2, 156.0, 174.0
18	212.1	cyclo (-Asn-Pro); cNP	70.1(Pro*, Asn**), 125.1, 153.1(derived from diketopiperazine rings)
19	201.1	pyroGlu-Ala	28.1(pyroGlu*), 41.4(pyroGlu*), 44.3(Ala*), 56.2(pyroGlu*), 84.1(pyroGlu*), 90.2(y1)
20	213.1	cyclo (-Asp-Pro); cDP	70.2(Pro*, Asp**), 125.0, 153.1(derived from diketopiperazine rings)
21	224.0	*cannot be assigned to peptide*	77.1, 104.1, 132.1, 143.9, 160.0, 188.0, 206.0
22	220.1	Pantothenic acid	30.2, 43.2, 57.1, 72.1, 90.1, 98.0, 124.1
23	201.1	cyclo(-Ser-Ile) or cyclo(-Ser-Leu); cSI/cSL	60.0(Ser*), 86.0(Ile*, Leu*), 153.0(derived from diketopiperazine rings)
24	208.1	*cannot be assigned to peptide*	72.1, 79.0, 85.7, 88.9, 108.8, 116.2, 132, 144.0, 153.0, 160.0
25	208.1	*cannot be assigned to peptide*	88.9, 106.9, 116.2, 128.1, 144.0, 160.0, 188.3
26	206.0	N-lactoyl-Asp	77.1 (lactoyl), 89.1(Asp*), 105.0, 132.0 (y1), 188.0, 206.0

(continued)

Table 1. *(continued)*

Peak	Precursor ion (*m/z*)	Estimated structure	Product ions (*m/z*)
27	219.1	cyclo (-Ala-Phe); cAF	44.1(Ala*), 120.0 (Phe*), 98.0 (derived from diketopiperazine rings)
28	211.1	cyclo (-Ile-Pro); cIP	70.2(Pro*, Ile**), 86.1(Ile*), 98.1 (derived from diketopiperazine rings)
29	211.1	cyclo (-Leu-Pro); cLP	70.2(Pro*, Leu**), 86.3(Leu*), 98.1(derived from diketopiperazine rings)
30	245.0	Uridine	43.1, 70.1, 84.1, 95.9, 113.0, 134.0
31	230.1	*cannot be assigned to peptide*	41.1, 69.1, 86.1
32	245.1	pyroGlu-Asp	41.3(pyroGlu*), 70.2(Asp**), 84.1(pyroGlu*), 125 (--), 181.0(y1)
33	227.1	pyroGlu-Pro	41.3(pyroGlu*), 56.2(pyroGlu*), 70.2(Pro*), 84.1(pyroGlu*, Glu**), 116.1(y1),
34	229.1	pyroGlu-Val	41.2(pyroGlu*), 55.2(Val*),72.1(Val*), 84.1 (pyroGlu*), 118.1(y1)
35	229.1	cyclo (-Asp-Leu); cDL	85.0 (Asp*), 86.2 (Leu*), 113.1 (derived from diketopiperazine rings)
36	238.1	*cannot be assigned to peptide*	41.1, 68.1, 84.0, 114.0, 142.0
37	243.1	pyroGlu-Ile	41.3(pyroGlu*), 44.0(Ile**), 56.2(pyroGlu*), 84.1(pyroGlu*), 86.1(Ile*), 132.0(y1)
38	243.1	pyroGlu-Leu	28.4(pyroGlu*), 41.3(pyroGlu*), 56.3(pyroGlu*), 84.1(pyroGlu*), 86.2(Leu*), 132.0(y1)
39	245.1	cyclo (-Phe-Pro); cFP	70.1(Pro*), 120.1(Phe*), 98.2 (derived from diketopiperazine rings)
40	259.1	Two pyroGlu	41.3(pyroGlu*), 56.2(pyroGlu*), 84.1(pyroGlu*), 130.0(y1)
41	259.1	pyroGlu-Glu	41.3(pyroGlu*), 56.3(pyroGlu*), 84.1(pyroGlu*), 102.1(Glu*), 130.1(z1), 148.0(y1)
42	251.1	cyclo (-Ser-Tyr); cSY	60.2 (Ser*), 136.0 (Tyr*), 98.0 (derived from diketopiperazine ring
43	260.1	*cannot be identified as peptide*	43.1, 67.0, 85.2, 114.1, 130.1, 139.9
44	261.1	*cannot be identified as peptide*	69.1, 84.1, 113.2, 141.0, 169.0, 197.1
45	261.1	cyclo (-Tyr-Pro); cYP	43.3, 70.0 (Pro*), 107, 136.2 (Tyr*), 98.0 (derived from diketopiperazine ring)
46	261.2	cyclo (-Phe-Ile/Leu); cFI/ cFL	86.1(Ile*), 120.1(Phe*), 113.0 (derived from diketopiperazine rings) 86.2(Leu*), 120.1(Phe*), 113.1 (derived from diketopiperazine rings)
47	256.0	*cannot be identified as peptide*	27.6, 43.2, 80.1, 110.9, 152, 180
48	275.1	*cannot be identified as peptide*	41.2, 68.1, 84.0, 97.0, 109.0, 130, 131.2, 239
49	293.1	pyroGlu-Tyr	41.4(pyroGlu*), 56.3(pyroGlu*), 84.1(pyroGlu*), 136.0(Tyr*)
50	277.1	pyroGlu-Phe	41.5(pyroGlu*), 56.1(pyroGlu*), 84.2(pyroGlu*), 120.1(Phe*), 166.0(y1)
51	295.1	cyclo (-Phe-Phe); cFF	120.2 (Phe*), 120.2 (Phe*), 98.0 (derived from diketopiperazine rings)

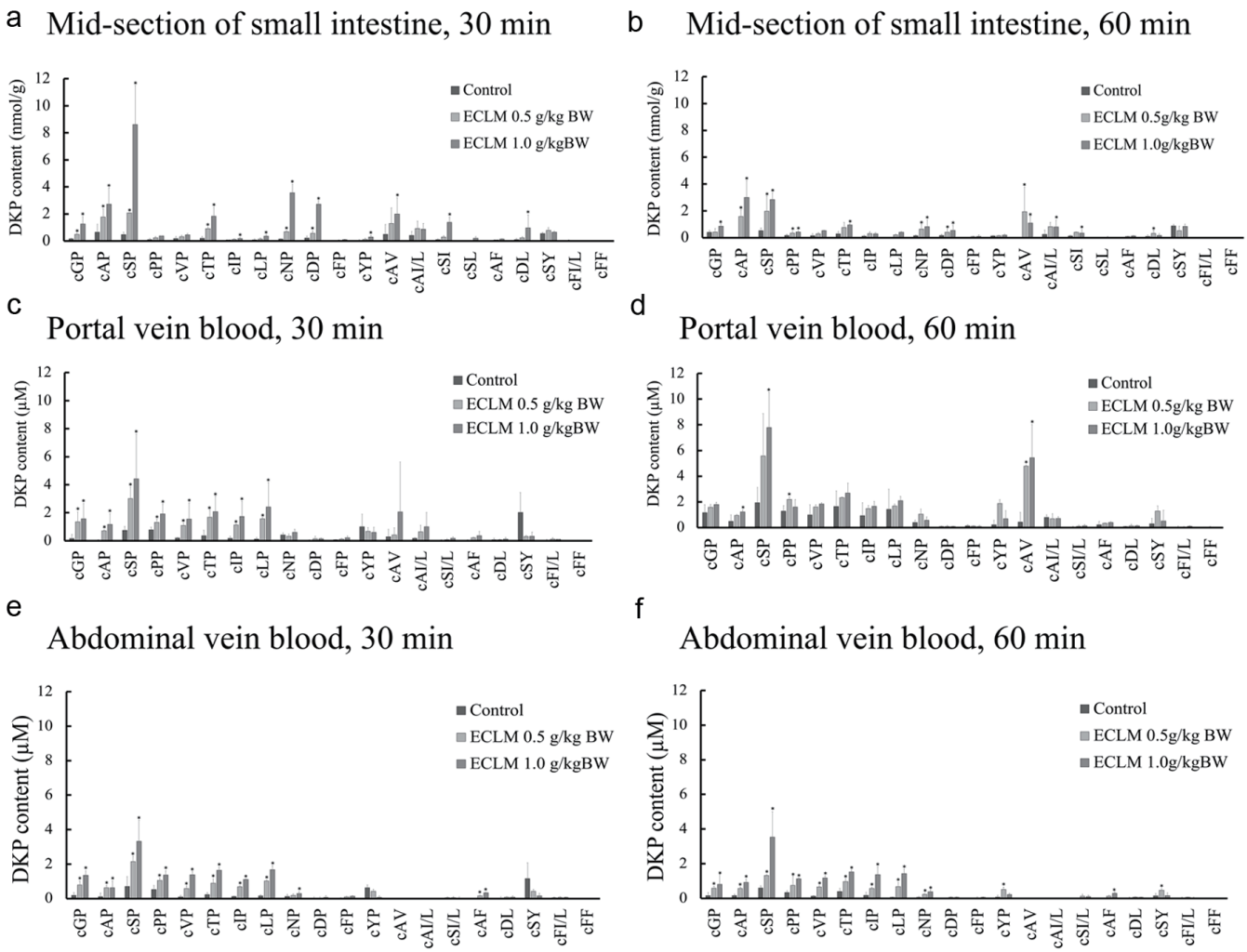

Figure 4. DKP levels in rat body 30 and 60 min after oral administration of ECLM (0.5 and 1.0 g/kg body weight). (a and b) Mid-section of the small intestine; (c and d) portal vein blood plasma; (e and f) abdominal vein blood plasma. Data are shown as mean ± SD (n = 3), *$p < 0.05$ (*t*-test). DKPs: cyclo-Gly-Pro [cGP], cyclo-Ala-Pro [cAP], cyclo-Ser-Pro [cSP], cyclo-Pro-Pro [cPP], cyclo-Val-Pro [cVP], cyclo-Thr-Pro [cTP], cyclo-Ile-Pro [cIP], cyclo-Leu-Pro [cLP], cyclo-Asn-Pro [cNP], cyclo-Asp-Pro [cDP], cyclo-Phe-Pro [cFP], cyclo-Tyr-Pro [cYP], cyclo-Ala-Val [cAV], cyclo-Ala-Ile [cAI], cyclo-Ala-Leu [cAL], cyclo-Ser-Ile [cSI], cyclo-Ser-Leu [cSL], cyclo-Ala-Phe [cAF], cyclo-Asp-Leu [cDL]), cyclo-Ser-Tyr [cSY], cyclo-Ile-Phe [cIF], cyclo-Leu-Phe [cLF], and cyclo-Phe-Phe [cFF],

for cAV. The levels of all DKPs in the abdominal vein blood were lower than those in portal blood. DKPs with high bioavailability can be classified as hydrophilic DKPs (cDP, cNP, cGP, cSP, and cTP), intermediate DKPs (cAP, cPP, and cAV), and hydrophobic DKPs (cDL, cIP, cLP, and cVP).

3.4. Effects of DKPs on cell viability

Overall, 12 DKPs (cDP, cNP, cGP, cSP, cTP, cAP, cPP, cAV, cIP, cLP, cVP, and cDL,) with high bioavailability were selected and mixed to give a final concentration 0.01, 0.1, 1.0 and 10.0 μM of each DKP. As shown in Figure 5, treatment of J774A.1 macrophages with the DKP mixture at various concentrations had no adverse effects on cell growth, indicating that the DKPs were non-toxic.

In contrast, treatment of J774A.1 macrophages with LPS at 0.1, 1.0, and 10.0 μg/mL led to a dose-dependent decrease in viability (76.1 ± 0.8%, 56.5 ± 1.8%, and 43.2 ± 2.0%, respectively). Co-treatment with the DKP mixture comprising of 1.0 μM of each DKP significantly restored cell viability to 98.3 ± 2.2%, 92.4 ± 2.1%, and 83.8 ± 2.5%, respectively. These findings indicate that DKPs exert a protective effect on J774A.1 under LPS-induced inflammatory conditions.

3.5. Effects of DKPs on NO production

Figure 6 presents nitrite levels in the medium of LPS-stimulated macrophages treated with the DKP mixtures, based on their bioavailability in the portal and abdominal blood, and small intestinal tissue. As shown in Figure 6a, NO production (nitrite) was monitored at 2, 4, 8, 12, 24, 36, and 48 h. All DKP mixtures-treated groups exhibited significant reductions in NO levels compared with the LPS-only group at 12 and 24 h. While NO levels increased over 36 h in all groups, this was possibly due to the metabolism and degradation of the DKPs after prolonged incubation. Therefore, we performed another experiment using the DKP mixtures at

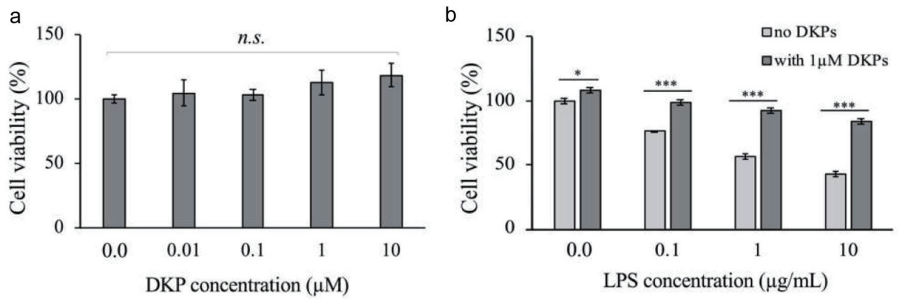

Figure 5. Effect of a diketopiperazine (DKP) mixture on the viability of J774A.1 cell. (a) Cells were treated with various concentrations of DKP mixture (0.01, 0.1, 1.0, and 10.0 μM of each DKP) for 24 h; (b) Cells were treated with lipopolysaccharides (LPS) alone (0.1, 1.0, and 10.0 μg/mL) or co-treated with 1 μM DKP mixture alongside each LPS concentration. Data are shown as mean ± SD (n = 3), *$p < 0.05$, **$p < 0.01$, ***$p < 0.001$ (*t*-test). *n.s.* represents no significant difference

different concentrations (0.1 μM and 1 μM) of each DKPs for 12 and 24 h. As shown in Figure 6b, all DKP mixtures significantly suppressed the LPS-induced NO production both at 12 and 24 h. There were no significant differences in NO levels between the negative control (no LPS) and all DKP mixture-treated groups.

As shown in Figure 6c, the DKPs were further grouped based on their hydrophobicity into hydrophilic (five DKPs), intermediate (three DKPs), and hydrophobic mixtures (four DKPs) mixtures.

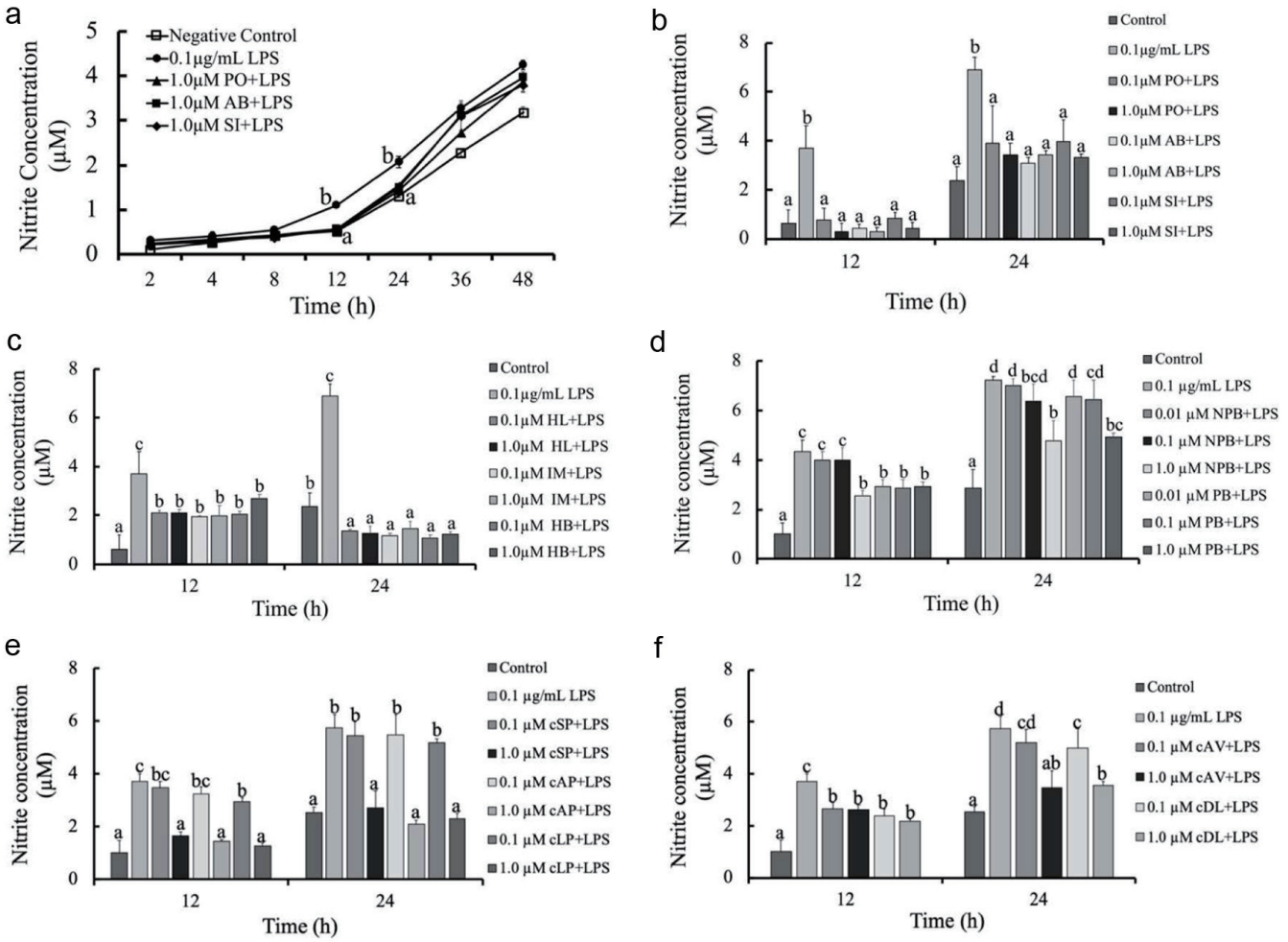

Figure 6. Effects of DKP mixtures on NO production in LPS-stimulated J774A.1 cells. (a and b) DKP mixtures based on bioavailability: PO, abundant in portal vein-blood DKPs; AB, abundant in abdominal vein-blood DKPs; and SI, abundant in mid-small intestine DKPs. (c) DKP mixtures based on hydrophobicity: HL, hydrophilic DKPs; IM, intermediate DKPs; and HB, hydrophobic DKPs. (d) DKP mixtures based on presence of proline: PB, proline-based DKPs; and NPB, non-proline-based DKPs. (e and f) Individual DKPs. Data are shown as mean ± SD (n = 3). Different letters (a-d) indicate significant differences between groups (Tukey's post hoc, $p < 0.05$). LPS, lipopolysaccharides

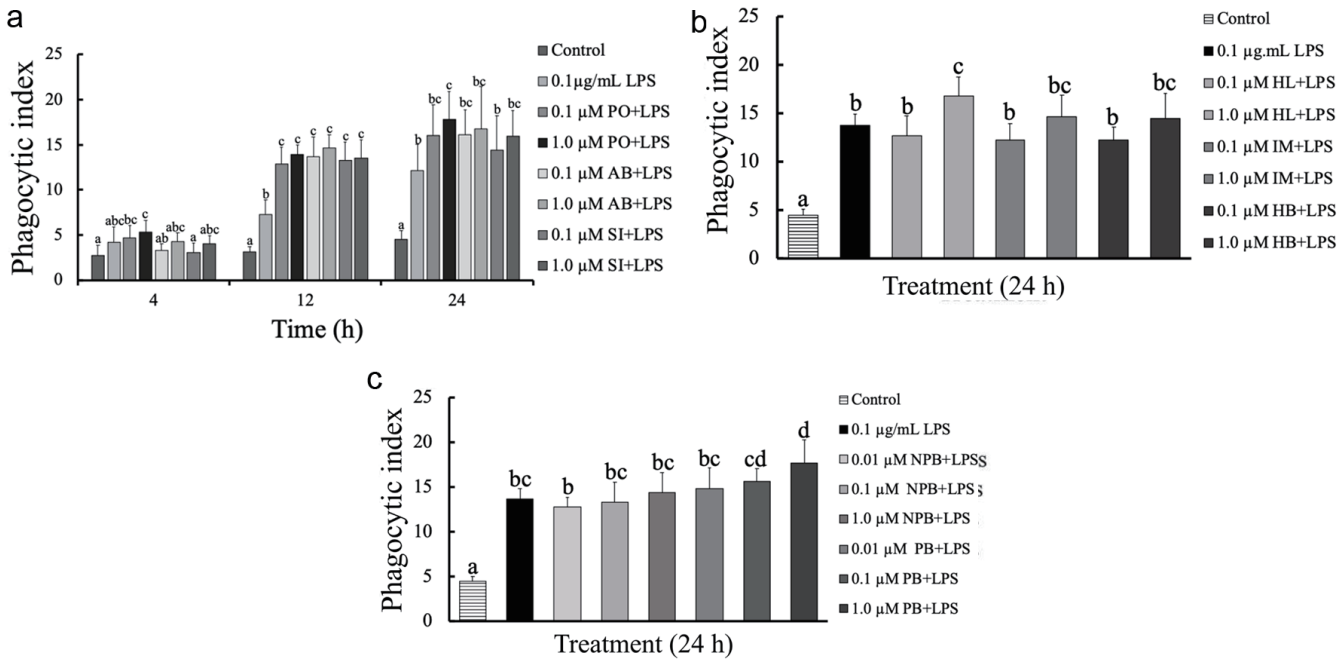

Figure 7. Effects of DKP mixture on phagocytosis in LPS-stimulated J774A.1 cells. (a) DKP mixtures based on bioavailability: PO, abundant in portal vein-blood DKPs; AB, abundant in abdominal vein-blood DKPs; and SI, abundant in mid-small intestine DKPs. (b) based on hydrophobicity: HL, hydrophilic DKPs; IM, intermediate DKPs; and HB, hydrophobic DKPs. (c) based on presence of proline: PB, proline-based DKPs; and NPB, non-proline-based DKPs. For PO, AB, and SI, refer to legend of Figure 6. Data are shown as mean ± SD (n = 3). Different letters (a-d) indicate significant differences between groups (Tukey's post hoc, $p < 0.05$). LPS, lipopolysaccharides

Treatments with the three groups of DKP mixtures at both doses significantly suppressed LPS-induced NO production at 12 and 24 h. However, there was no significant difference in NO levels among the three groups, indicating that the hydrophobicity of DKPs was not crucial for suppressing LPS-induced NO production.

It has been reported that DKPs are more easily generated from proline-containing peptides due to their three-dimensional structure (Otsuka et al., 2019). DKPs abundantly (≥1μM) found in the body after ingestion of aqueous extract of ECLM were also grouped into proline–based DKPs (PB: cSP, cAP, and cLP) and non-proline–based DKPs (NPB: cAV, and cDL). As shown in Figure 6d, PB-DKPs consistently suppressed NO production at 12 h at all concentrations than the LPS-only group. No significant differences were observed among the concentrations. At 24 h, PB-DKPs at 0.01 and 0.1 μM of each DKP did not significantly reduce the LPS-induced NO production; however, 1.0 μM PB-DKPs significantly reduced NO production (Figure 6a–c). NPB-DKPs at 0.01 and 0.1 μM showed no significant reduction in NO production at either 12 or 24 h, whereas only the 1.0 μM NPB-DKPs group showed moderate suppression at both time points.

Furthermore, individual DKPs that were abundantly present in the body after ECLM administration were tested. As shown in Figure 6e, 0.1 μM PB-DKPs (cSP, cAP, and cLP) did not significantly reduce NO production at either 12 or 24 h. However, at 1.0 μM, all three significantly inhibited LPS-induced NO production. Figure 6f shows that individual NPB-DKPs significantly suppressed LPS-induced NO production at both concentrations after 12 h; however, no dose-dependent response was observed, and the values were significantly higher than those of the negative control without LPS stimulation. On the other hand, 1.0 μM of individual PB-DKPs reduced NO production until it was no longer significantly different from the negative control after 12 h. At 24 h, individual NPB-DKPs showed an inhibitory pattern similar to that of the individual PB-DKPs.

3.7. Effects of DKPs on phagocytosis

As shown in the Figure S1, approximately 95% of J774A.1 cells that did not receive LPS and DKPs treatments (negative control) engulfed fewer than three beads, whereas approximately 20% of LPS-stimulated cells engulfed more than four beads. The percentage of cells engulfing four or more beads was used as the phagocytic index. The phagocytosis-enhancing activities of DKP mixtures–classified based on bioavailability, hydrophobicity, and the presence of proline, and individual DKPs were evaluated (Figures 7). Phagocytosis was assessed at 4, 12, and 24 h after treatment with 0.1 or 1.0 μM concentrations of DKPs abundantly present in portal (PO), abdominal blood (AB), and mid-section of small intestine (SI). After 4 h, only treatment with LPS and PO-DKP mixture significantly increased the phagocytic index compared with that of the negative control (Figure 7a). At 12 h, all DKP mixtures significantly enhanced the phagocytic index relative to that of the LPS-only group, with no significant differences among the mixtures. At 24 h, only the 1.0 μM PO-DKP mixture maintained a significant increase in phagocytic index.

The phagocytic activity of the hydrophilic (HL; five DKPs), intermediate (IM; three DKPs), and hydrophobic (HB; four DKPs) mixtures in the presence of LPS was examined 24 h after treatment with 0.1 and 1.0 μM of each DKP in the mixture. Treatment did not result in significant changes in phagocytic index compared to LPS-only treatment, except for treatment with 1 μM HL (Figure 7b). Similarly, only treatment with 1.0 μM of the proline–based (PB) DKP mixture significantly increased phagocytic index (Figure 7c). In contrast, non-

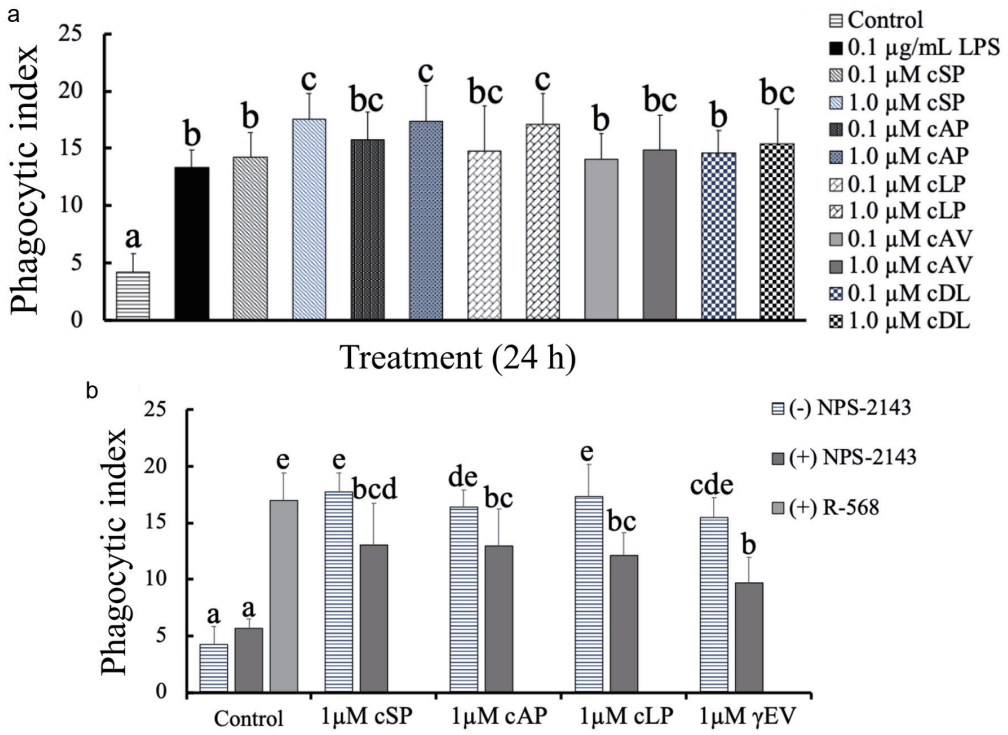

Figure 8. Effects of individual DKPs on phagocytosis in LPS-stimulated (a) and non-LPS–stimulated J774A.1 cells (b). (a) LPS–stimulated phagocytosis in cells treated with five highly bioavailable DKPs. (b) Non-LPS–stimulated phagocytosis in cells treated with three proline-based DKPs (1µM). Involvement of CaSR was assessed by pre-treatment with the CaSR antagonist, NPS-2143, and agonist, R-568. Data are shown as mean ± SD. Different letters (a-e) indicate significant differences between groups (Tukey's post hoc, $p < 0.05$). LPS, lipopolysaccharides; cSP, cyclo-Ser-Pro; cAP, cyclo-Ala-Pro; cLP, cyclo-Leu-Pro; γ-EV, γ -Glu-Val.

proline–based (NPB) DKPs did not have any significant effects.

The effects of individual DKPs on phagocytic activity in the presence of LPS 24 h after treatment were examined (Figure 8a). At 0.1 µM, neither PB-DKPs (cSP, cAP, cLP) nor NPB-DKPs (cDL, cAV) significantly altered the phagocytic index relative to the LPS-only treatment. However, at 1.0 µM, all PB-DKPs significantly enhanced the phagocytic index in LPS-stimulated macrophages, whereas NPB-DKPs did not. These findings indicated that the presence of proline within DKPs enhanced phagocytosis in LPS-stimulated macrophages.

To test whether DKPs can act under non-inflammatory conditions, three PB-DKPs (cSP, cAP, and cLP) were applied to macrophages in the absence of LPS. These DKPs increased phagocytosis even in the absence of LPS, suggesting that DKPs promote phagocytosis via a pathway other than that mediated by LPS (Figure 8b). Treatment with R-568, a CaSR allosteric agonist, significantly increased phagocytosis. Additionally, NPS-2143, a CaSR antagonist, significantly reduced DKP-induced enhancement of phagocytosis. However, DKP-induced phagocytosis was not completely inhibited by the CaSR antagonist. For further confirmation, the effect of γ-glutamyl valine (γ-EV), a known CaSR activator, on phagocytic activity was tested. γ-EV also enhanced phagocytosis and its activity was reduced by the CaSR antagonist (NPS-2143). These findings indicate that DKPs found in ECLM enhance phagocytosis in J774A.1 at least partially via the allosteric activation of CaSR.

3.8. Effects of DKPs on LPS-stimulated IL-6 protein secretion

Individual DKPs—cSP, cAP, cLP, cAV, cDL—at a physiologically relevant concentration (1 µM) significantly attenuated IL-6 secretion by LPS-stimulated macrophages (Figure 9). At 2 h, a very minimal and negligible increase in IL-6 levels was observed in LPS-stimulated cells treated with R-568, a known CaSR allosteric activator, whereas IL-6 were not detected (n.d.) in DKP-treated samples. At 6 h after LPS stimulation, all DKP-treated macrophages showed a significant reduction in IL-6 levels compared to LPS-treated macrophages. cLP exhibited the strongest suppression. Similarly, R-568 treatment also reduced IL-6 levels under LPS stimulation, supporting the possible involvement of CaSR-mediated signaling in the anti-inflammatory effects of DKPs.

4. Discussion

ECLM is a standardized extract from the mycelium of the shiitake mushroom (*Lentinula edodes*) that has been used in numerous human clinical trials in patients suffering from cancer and viral infections yielding positive results. Providing healthy individuals with ECLM supplements enhances the number and function of natural killer (NK) cells and T cells, suggesting an immune-enhancing effect (Shin et al., 2019). Further, ECLM alleviates chemotherapy-induced side effects and improves liver function in patients with liver cancer, which has been attributed to its anti-inflammatory properties (Matsui et al., 2002; Cowawintaweewat et al., 2006; Daddaoua et al., 2007; Tanaka et al., 2014). It is well known that immune responses are typically initiated by acute inflammatory signals mediated by macrophages and other innate immune cells, whereas chronic inflammation, especially macrophage-mediated inflammation, can exacerbate pathologies such as hepatitis (Kim

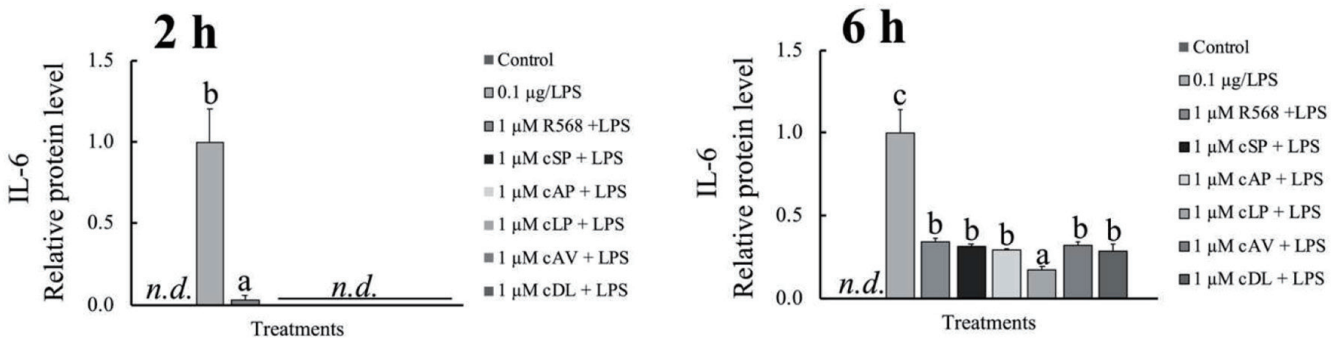

Figure 9. Effects of individual DKPs on interleukin (IL)-6 protein in medium of LPS-stimulated cells. Data are shown as mean ± SD. Different letters (a–c) indicate significant differences between groups (Tukey's post hoc, $p < 0.05$). *n.d.* represents not detected. LPS, lipopolysaccharides; cSP, cyclo-Ser-Pro; cAP, cyclo-Ala-Pro; cLP, cyclo-Leu-Pro; cAV, cyclo-Ala-Val; cDL, cyclo-Asp-Leu

and Lee, 2025). Therefore, their immunostimulatory and anti-inflammatory effects are contradictory. However, under normal physiological conditions, both immune and inflammatory responses coexist in the human body.

In an earlier study, we have shown that an aqueous extract of ECLM inhibits IL-1β–induced NO production from hepatocytes, and that adenosine is involved in anti-inflammatory responses (Tanaka et al., 2014). The present study demonstrates a new function of ECLM, wherein the aqueous extract of ECLM promotes macrophage phagocytosis, thereby having potentially enhancing innate immunity. Fungal polysaccharides, such as β-glucans, are generally considered to act as ligands for toll-like receptor (TLR) 2/4 and can induce phagocytosis even in the absence of LPS stimulation (Snarr et al., 2017). Crude ECLM has been reported to activate cytokines and chemokines secretion in monocytes via toll-like receptor 4/myeloid differentiation primary response 88 (TLR4/MyD88) and nuclear factor kappa-light-chain enhancer of activated B cells/ mitogen-activated protein kinases (NF-κB/MAPK) pathways (Daddaoua et al., 2013), thereby priming other innate immune cells through interferon (IFN)-γ and IL-17 production (Lee et al., 2012). Indeed, ECLM contains polysaccharides, such as α- and β-glucans, which have been associated with immunomodulatory activity (Mallet et al., 2016; Mathew et al., 2017). However, when the aqueous extract of ECLM was fractionated by ethanol precipitation, the soluble fraction–rather than the precipitate fraction–showed stronger phagocytosis-enhancing activity. The soluble and precipitate fractions consisted of low– and high–molecular weight compounds, such as polysaccharides, respectively. These results indicate that low–molecular weight compounds, rather than glucans, in ECLM play a key role in phagocytosis-enhancing activity. At least 23 DKPs were identified in the active fraction. After oral administration of ECLM (1 g/kg body weight) in rats, some DKPs reached concentrations exceeding 1 μM in portal and abdominal blood. The doses (0.5 and 1g/kg) for rats is equivalent to 80 and 161 mg/kg for humans by conversion based on body surface area (Nair and Jacob, 2016). Thus, it can be anticipated that some DKPs in ECLM can reach μM levels in human blood after ingestion of realistic doses. However, The ADME of DKPs after ECLM ingestion in humans should be investigated.

The presence of DKPs in the blood circulation indicates resistance to proteolysis during digestion, likely due to their rigid cyclic structure, which allows them to reach systemic circulation (Otsuka et al., 2019, 2020). At 12 h after stimulation with three highly bioavailable mixtures of DKPs (each DKP present at concentrations of 0.1 and 1 μM), phagocytosis in LPS-stimulated macrophages was significantly enhanced, which suggests that ECLM ingestion may deliver sufficient amounts of DKPs to promote phagocytosis under inflammatory conditions. Present data clearly indicate that low molecular weight DKPs rather than α- and β-glucans play crucial role in enhancing phagocytosis in macrophages.

Mixtures of highly bioavailable DKPs (eight or nine types) showed higher phagocytosis-enhancing activity under LPS stimulation than individual DKPs, whereas differences in DKP structure had a relatively small effect on phagocytosis-enhancing activity. This suggests that DKPs in the ECLM have additive effects; therefore, even relatively minor DKPs in the ECLM contribute to its phagocytosis-enhancing activity. DKPs are naturally present in a wide range of fermented products with a long history of presence across various foods, such as fermented soybean paste (*miso*) and fish sauce (Nagao et al., 2024; Rahmadian et al., 2025). These foods are generally recognized as safe and serve as dietary sources of many modified peptides, including DKPs. For example, a typical serving of *miso* (10 g) contains approximately 20–30 μmol of total DKPs, whereas one serving of fish sauce (10 mL) provides about 100–500 μmol. Interestingly, ECLM contains DKPs at levels remarkably higher than those found in traditional fermented foods—estimated to be 10- to 50-fold greater than in *miso*, reaching up to 1,000 μmol of total DKPs per 10 g of ECLM. ECLM also contains significantly less salt than fermented foods, making it a rich and diverse source of DKPs, the intake of which is not limited by salt content.

It is well known that phagocytosis in macrophages is enhanced by LPS through the classical TLR4–NF-κB/MAPK pathways (Chen et al., 2023). Activation of this pathway leads to phosphorylation of p38 and extracellular signal-regulated kinase (ERK), which promotes cytoskeletal rearrangement, thereby enhancing phagocytosis. At the same time, TLR4–NF-κB/MAPK signaling induces the production of proinflammatory cytokines like IL-6 and enzymes such as inducible nitric oxide synthase (iNOS), resulting in increased NO production. However, in our study, DKPs reduced LPS-induced NO and IL-6 production, suggesting that DKPs suppress TLR4–NF-κB/MAPK pathway. Therefore, DKPs modulate macrophage function through alternative signaling mechanisms distinct from the canonical TLR4–NF-κB/MAPK pathway. Interestingly, Chee et al. (2017) reported that another food-derived peptide, γ-EV, suppresses TNF-α–induced inflammation via the CaSR.

The classical function of the CaSR is thought to be the sensing of extracellular calcium ions and regulation of calcium ion homeostasis (Chu et al., 2022). In the classical intracellular signaling of CaSR, extracellular calcium ions activate CaSR, which triggers the intracellular G-protein–mediated pathway, in which Gαq/11 acti-

vates phospholipase C (PLC), leading to the generation of inositol 1, 4, 5-trisphosphate (IP3) and diacylglycerol (DAG) (Chu et al., 2022). IP3 stimulates Ca^{2+} release from the endoplasmic reticulum and activates calmodulin-dependent protein kinases, whereas DAG and Ca^{2+} activate protein kinase C (PKC), together down-regulating parathyroid hormone (PTH) secretion in parathyroid cells. CaSR is also distributed in other cells, such as macrophages, and promotes MAPK signaling, including the phosphorylation of ERK, which drives proinflammatory responses. Activation of the CaSR has been reported to enhance innate immune functions (Iamartino and Brandi 2022). This process can be blocked by the CaSR allosteric antagonist NPS-2143. On the other hand, CaSR has another intracellular pathway, namely β-arrestin-2 pathway. In this pathway, CaSR is phosphorylated by G-protein receptor kinases (GRKs), creating docking sites for β-arrestin-2. Binding β-arrestin-2 to CaSR desensitizes G-protein signaling and redirects signaling toward the β-arrestin-2–dependent pathway. β-Arrestin-2 interacts with the transforming growth factor β-activated kinase 1 (TAK1)-binding protein (TAB1), thereby interfering with TAK1 activation and suppressing downstream NF-κB/MAPK signaling. Chee et al. (2017) concluded that γ-EV shifts the immune response away from proinflammatory G-protein signaling toward β-arrestin-2–mediated signaling (biased activation of CaSR), consequently attenuating inflammatory responses through allosteric activation of CaSR.

The present study revealed that the phagocytosis-enhancing activity of DKPs was partially abolished by the CaSR antagonist, NPS-2143. In addition, CaSR agonists, R-568 and γ-EV, enhanced the macrophage phagocytosis. These suggest that CaSR may be involved in the immunomodulatory effects of DKPs. CaSR-bound β-Arrestin-2 also functions as a scaffold protein that can link CaSR to signaling molecules, such as Src, Akt, and ERK, which phosphorylate them. p-Src phosphorylates the immunoreceptor tyrosine–based activation motifs (ITAMs) of Fcγ receptors on the macrophage surfaces, leading to cytoskeletal rearrangement and enhanced phagocytosis (Bournazos et al., 2020). Based on the present findings and earlier reports, we propose a mechanism for the immunomodulatory effects of DKPs. Similar to γ-EV, DKPs biasedly activate CaSR and following β-arrestin-2 pathway, which suppresses LPS-induced NO and IL-6 productions by suppressing LPS-TLR4-NF-κB/MAPK signaling and may enhance Src activation and phagocytosis. DKPs also suppress LPS-TLR4-NF-κB/MAPK–induced phagocytosis but can enhance phagocytosis via the β-arrestin-2 pathway and simultaneously suppress NO and IL-6 productions. As shown in Figure 8, the enhancement of phagocytosis by DKPs can at least compensate for or proceed with LPS-induced phagocytosis. It is worthy to mention that DKPs show higher bioavailability than γ-EV, another food-derived CaSR agonist (Rahmadian1 et al., 2025).

5. Conclusion

ECLM contains highly bioavailable and bioactive DKPs, which suppress LPS-induced NO and IL-6 productions; however, DKPs enhance phagocytosis in macrophages by biased activation of CaSR, which tune inflammatory response via the G protein pathway to anti-inflammatory and phagocytic responses via the β-arrestin-2 pathway. Thus, ECLM ingestion can enhance immunity without increasing the inflammatory response. However, further studies are required to elucidate the underlying molecular mechanisms. We should also evaluate whether the dual immunomodulatory effects of DKPs are mediated by macrophage differentiation. Future in vivo studies should also assess the phagocytosis-enhancing activity of ECLM and DKPs, particularly in the context of dietary supplementation, to strengthen the evidence of their immunomodulatory potential.

Acknowledgments

This work was supported by Commissioned Research between Kyoto University and Amino Up Co. Ltd. (Project number: 150221000026).

Data availability

The authors declare that data supporting the findings of this study are available in this article.

Supplementary material

Figure S1. Numbers of beads in macrophages treated with vehicle and LPS.

References

Aito-Inoue, M., Ohtsuki, K., Nakamura, Y., Park, E.Y., Iwai, K., and Morimatsu, F. (2006). Improvement in isolation and identification of food-derived peptides in human plasma based on precolumn derivatization of peptides with phenyl isothiocyanate. J. Agric. Food Chem. 54(15): 5261–5266.

Asai, T.T., Oikawa, F., Yoshikawa, K., Inoue, N., and Sato, K. (2020). Food-derived collagen peptides, prolyl-hydroxyproline (Pro-Hyp), and hydroxyprolyl-glycine (Hyp-Gly) enhance growth of primary cultured mouse skin fibroblast using fetal bovine serum free from hydroxyprolyl peptide. Int. J. Mol. Sci. 21(1): 229.

Bidlingmeyer, B.A., Cohen, S.A., and Tarvin, T.L. (1984). Rapid analysis of amino acids using pre-column derivatization. J. Chromatogr. 336: 93–104.

Bournazos, S., Gupta, A., and Ravetch, J.V. (2020). The role of IgG Fc receptors in antibody-dependent enhancement. Nat. Rev. Immunol. 20(11): 633–643.

Chee, M.E., Majumder, K., and Mine, Y. (2017). Intervention of dietary dipeptide gamma-l-glutamyl-l-valine (γ-EV) ameliorates inflammatory response in a mouse model of LPS-induced sepsis. J. Agric. Food Chem. 65(29): 5953–5960.

Chen, S., Saeed, A.F.U.H., Liu, Q., Jiang, Q., Xu, H., Xiao, G.G., Rao, L., and Duo, Y. (2023). Macrophages in immunoregulation and therapeutics. Signal Transduct. Target. Ther. 8: 207.

Chowdhury, A.H., Cámara, M., Verma, C., Eremin, O., Kulkarni, A.D., and Lobo, D.N. (2019). Modulation of T regulatory and dendritic cell phenotypes following ingestion of Bifidobacterium longum, AHCC® and azithromycin in healthy individuals. Nutrients 11(10): 2470.

Chu, H., Qin, Z., Ma, J., Xie, Y., Shi, H., Gu, J., and Shi, B. (2022). Calcium-Sensing Receptor (CaSR)-Mediated Intracellular Communication in Cardiovascular Diseases. Cells 11(19): 3075.

Cowawintaweewat, S., Manoromana, S., Sriplung, H., Khuhaprema, T., Tongtawe, P., Tapchaisri, P., and Chaicumpa, W. (2006). Prognostic improvement of patients with advanced liver cancer after active hexose correlated compound (AHCC) treatment. Asian Pac. J. Allergy Immunol. 24(1): 33–45.

Daddaoua, A., Martínez-Plata, E., López-Posadas, R., Vieites, J.M., González, M., Requena, P., Zarzuelo, A., Suárez, M.D., Sánchez de Medina, F., and Martínez-Augustin, O. (2007). Active hexose correlated compound acts as a prebiotic and is anti-inflammatory in rats with hapten-induced colitis. J. Nutr. 137(5): 1222–1228.

Daddaoua, A., Martínez-Plata, E., Ortega-González, M., Ocón, B., Aranda, C.J., Zarzuelo, A., Suárez, M.D., Sánchez de Medina, F., and Martínez-Augustin, O. (2013). The nutritional supplement Active Hexose Correlated Compound (AHCC) has direct immunomodulatory actions on intestinal epithelial cells and macrophages involving TLR/MyD88 and NF-κB/MAPK activation. Food Chem. 136(3-4): 1288–1295.

Dash, S.P., Gupta, S., and Sarangi, P.P. (2024). Monocytes and macrophages: Origin, homing, differentiation, and functionality during inflammation. Heliyon 10(8): e29686.

Iamartino, L., and Brandi, M.L. (2022). The calcium-sensing receptor in inflammation: Recent updates. Front. Physiol. 13: 1059369.

Kawaguchi, Y. (2009). Improved survival of patients with gastric cancer or colon cancer when treated with active hexose correlated compound (AHCC): Effect of AHCC on digestive system cancer. Nat. Med. J. 1(1): 1–6.

Kim, H., Kim, J.-H., and Im, J.-A. (2014). Effect of active hexose correlated compound (AHCC) in alcohol-induced liver enzyme elevation. J. Nutr. Sci. Vitaminol. 60(5): 348–356.

Kim, M.E., and Lee, J.S. (2025). Advances in the regulation of inflammatory mediators in nitric oxide synthase: Implications for disease modulation and therapeutic approaches. Int. J. Mol. Sci. 26(3): 1204.

Kogiso, M., Wakame, K., Sakai, T., Yamamoto, S., Sundaresan, A., and Kulkarni, A.D. (2015). Active hexose correlated compound and T cell response in hind-limb-unloaded BALB/c mice. Int. J. Surg. Res. 2: 32–38.

Lee, W.W., Lee, N., Fujii, H., and Kang, I. (2012). Active Hexose Correlated Compound promotes T helper (Th) 17 and 1 cell responses via inducing IL-1β production from monocytes in humans. Cell Immunol. 275(1-2): 19–23.

Mallet, J.F., Graham, É., Ritz, B.W., Homma, K., and Matar, C. (2016). Active Hexose Correlated Compound (AHCC) promotes an intestinal immune response in BALB/c mice and in primary intestinal epithelial cell culture involving toll-like receptors TLR-2 and TLR-4. Eur. J. Nutr. 55(1): 139–46.

Mathew, L., Gaikwad, A., Gonzalez, A., Nugent, E.K., and Smith, J.A. (2017). Evaluation of active hexose correlated compound (AHCC) in combination with anticancer hormones in orthotopic breast cancer models. Integr. Cancer Ther. 16(3): 300–307.

Matsui, Y., Uhara, J., Satoi, S., Kaibori, M., Yamada, H., Kitade, H., Imamura, A., Takai, S., Kawaguchi, Y., Kwon, A.H., and Kamiyama, Y. (2002). Improved prognosis of postoperative hepatocellular carcinoma patients when treated with functional foods: A prospective cohort study. J. Hepatol. 37(1): 78–86.

Nagao, A., Nakamoto, Y., Miyauchi, S., and Sato, K. (2024). Presence of modified peptides with high bioavailability and angiotensin-converting enzyme inhibitory activity in Japanese fermented soybean paste (miso). J. Agric. Food Chem. 72: 18942–18956.

Nair, A.B., and Jacob, S. (2016). A simple practice guide for dose conversion between animals and human. J Basic Clin Pharm. 7(2): 27–31.

Otsuka, Y., Arita, H., Sakaji, M., Yamamoto, K., Kashiwagi, T., Shimamura, T., and Ukeda, H. (2019). Investigation of the formation mechanism of proline-containing cyclic dipeptide from the linear peptide. Biosci. Biotechnol. Biochem. 83(12): 2355–2363.

Otsuka, Y., Shimamura, T., Sakaji, M., Arita, H., Kashiwagi, T., and Ukeda, H. (2020). Quantification of proline-containing cyclic dipeptides by LC-MS/MS. Anal. Sci. 36(8): 977–980.

Papayannopoulos, I.A. (1995). The interpretation of collision-induced dissociation tandem mass spectra of peptides. Mass Spectrom. Rev. 14: 49–73.

Rahmadian, Y., Miyauchi, S., Wijanarti, S., Asai, T., and Sato, K. (2025). Presence of γ-glutamyl 1 and β-aspartyl isopeptides, diketopiperazines, pyroglutamyl peptides, in addition to normal peptides in fish and soy sauces: Structures, contents and their bioavailability. J. Food Bioact. 29: 60–76.

Ritz, B.W., Nogusa, S., Ackerman, E.A., and Gardner, E.M. (2006). Supplementation with active hexose correlated compound increases the innate immune response of young mice to primary influenza infection. J. Nutr. 136(11): 2868–2873.

Sato, K., and Kashimoto, M. (2017). Profile summary of AHCC: Composition. In: Kulkarni, A.D., Calder, P.C., and Ito, T. (Ed.). Clinician's guide to AHCC. International Congress on Nutrition and Integrative Medicine, pp. 24–33.

Shin, M.S., Park, H.-J., Maeda, T., Nishioka, H., Fujii, H., and Kang, I. (2019). The effects of AHCC®, a standardized extract of cultured Lentinula edodes mycelia, on natural killer and T cells in health and disease: Reviews on human and animal studies. J. Immunol. Res. 2019: 3758576.

Singh, A., Adam, A., Rodriguez, L., Peng, B.-H., Wang, B., Xie, X., Shi, P.-Y., Homma, K., and Wang, T. (2023). Oral supplementation with AHCC®, a standardized extract of cultured Lentinula edodes mycelia, enhances host resistance against SARS-CoV-2 infection. Pathogens 12(4): 554.

Smith, J.A., Gaikwad, A.A., Mathew, L., Rech, B., Faro, J.P., Lucci, J.A., Bai, Y., Olsen, R.J., and Byrd, T.T. (2022). AHCC® supplementation to support immune function to clear persistent human papillomavirus infections. Front. Oncol. 12: 881902.

Snarr, B.D., Qureshi, S.T., and Sheppard, D.C. (2017). Immune recognition of fungal polysaccharides. J. Fungi 3(3): 47.

Tanaka, Y., Ohashi, S., Ohtsuki, A., Kiyono, T., Park, E.Y., Nakamura, Y., Sato, K., Oishi, M., Miki, H., Tokuhara, K., Matsui, K., Kaibori, M., Nishizawa, M., Okumura, T., and Kwon, A.H. (2014). Adenosine, a hepato-protective component in active hexose correlated compound: Its identification and iNOS suppression mechanism. Nitric Oxide 40: 75–86.

Terakawa, N., Matsui, Y., Satoi, S., Yanagimoto, H., Takahashi, K., Yamamoto, T., Yamao, J., Takai, S., Kwon, A.H., and Kamiyama, Y. (2008). Immunological effect of active hexose correlated compound (AHCC) in healthy volunteers: A double-blind, placebo-controlled trial. Nutr. Cancer 60(5): 643–651.

Wu, J., Sun, X., and Jiang, P. (2024). Metabolism-inflammasome crosstalk shapes innate and adaptive immunity. Cell Chem. Biol. 31(5): 884–903.

Yin, Z., Fujii, H., and Walshe, T. (2010). Effects of active hexose correlated compound on frequency of CD4+ and CD8+ T cells producing interferon-γ and/or tumor necrosis factor-α in healthy adults. Hum. Immunol. 71: 1187–1190.